ELSEVIER

Journal of Nuclear Materials 241–243 (1997) 82–91

journal of nuclear materials

Particle exhaust in radiative divertor experiments

H.-S. Bosch *, D. Coster, R. Dux, C. Fuchs, G. Haas, A. Herrmann, S. Hirsch, A. Kallenbach, J. Neuhauser, R. Schneider, J. Schweinzer, M. Weinlich, ASDEX Upgrade team, NBI team

Max-Planck-Institut für Plasmaphysik, EURATOM-IPP Association, D-85748 Garching Germany

Abstract

Power exhaust is one of the critical questions to be solved for ITER, especially with the side condition of sufficient particle exhaust. Since the H-mode threshold might require a high power flux over the separatrix, only small power losses inside the bulk plasma might be permitted, and thus eventually a large fraction of the power must be removed in the scrape-off layer and divertor plasma. Neutral energy losses can only remove a small fraction of the power, and therefore most of the power flux has to be radiated, either by hydrogen isotopes, by the intrinsic impurities (mainly carbon) or by additionally seeded impurities. However, all these scenarios with reduced power flow to the divertor imply also a reduced particle flow into the divertor. This might be critical for particle exhaust, especially concerning the helium ash. Reduction of the power flow to the divertor by enhanced radiation losses has been investigated in the large divertor experiments like JET, DIII-D, ASDEX Upgrade, and JT-60U, and an experimental overview of the present status will be given in this paper, together with a discussion of impurity exhaust (mainly He and Ne) in these scenarios.

Keywords: Poloidal divertor; Impurity transport; Improved confinement mode; Helium exhaust and control; Active pumping

1. Introduction

One of the most critical questions to be solved for ITER is the power exhaust problem. With a fusion power of 1.5 GW (80% and 20% of this power divided in neutrons and α-particles respectively) and 100 MW of auxiliary heating power, about 400 MW have to be exhausted from the plasma. With 100 MW radiated in the main plasma by Bremsstrahlung, 300 MW will still flow across the separatrix into the scrape-off layer (SOL), resulting in a peak power load on the divertor target plates in the order of 30 MW/m^2 [1]. The technically feasible limit for stationary operation, however, is about 5 MW/m^2. Therefore additional radiation losses are required to decrease the power flow to the target. Increased radiation losses may be induced by puffing of deuterium/tritium (i.e., the plasma species itself) or by seeding the plasma with additional impurities.

However, there are two side conditions to this problem: to reach ignition, ITER will have to operate in an improved confinement mode, and the only stationary scenario up to now is the H-mode with type-I ELMs. These type-I ELMs [2] result in short, very strong power and particle bursts on the divertor target plate, which are not tolerable for ITER. Therefore not only has the time averaged power flow to the divertor to be limited, but also type-I ELMs have to be avoided. H-mode operation also requires the power flow across the separatrix to be above the H–L threshold power [3], limiting the tolerable power loss in the core plasma. Therefore, radiation in the scrape-off layer and divertor plasma will be a necessary requirement for successful operation of the ITER divertor.

Reducing the power flow in the scrape-off layer strongly will result in detachment of the divertor plasma from the target plates [4]. In this state the electron temperature is about 1 eV (avoiding any problem with physical sputtering), the plasma pressure in front of the target plates is strongly reduced compared to the values at the mid plane, and also the ion flux to the target plate is strongly reduced. The latter, however, may cause problems concerning particle exhaust.

* Corresponding author.

PII S0022-3115(96)00497-7

The second side-condition to the power exhaust problem in ITER is the question of sufficient particle exhaust. The most stringent requirement is set by the fusion-produced helium, as its production rate is directly linked to the fusion power. With 1.5 GW fusion power 5.31×10^{20} α-particles are created per second which have to be exhausted as 'helium ash'. This is an absolute requirement, as He accumulation in the plasma would prevent steady state burning by dilution of the plasma and by its radiation losses [5]. Also the plasma species (D and T) and any seeded impurities have to be exhausted, but their exhaust rate is linked to the gas input, and is not considered a problem. However, sufficient exhaust means for all species that there has to be a particle flow to the pump entrance (divertor chamber), and if the ion flow to the target plates is eliminated in detached plasmas, this might be a problem.

In this paper we will first describe divertor scenarios with deuterium puffing and with additional impurity seeding, and compare these scenarios with respect to their particle exhaust characteristics.

2. Deuterium puffing

The first experiments with additional D_2-puffing in H-mode plasma with type-I ELMs were performed in DIII-D, and showed a strong reduction in the peak power load on the divertor target plate [6]. Between ELMs the plasma detaches close to the outer separatrix, but during the ELMs it reattaches [7]. This mode of operation is called Partially Detached Divertor (PDD) in DIII-D [8]. However, this scenario is not due to increased neutral losses, but due to radiation. Later experiments demonstrated clearly that the plasma detaches from the target plate due to increased radiation losses that are concentrated at or near to the X-point [7,9]. In general it has been found that the main radiating species in such a scenario is carbon, which, due to its radiation characteristics, tends to causes MARFEs. Although such experiments can be performed stationarily, an inherent problem is the uncontrollable steady influx of carbon due to physical and chemical sputtering at the walls and divertor target plates. Alcator C-mod always operates at rather high density and easily achieves detachment in Ohmically heated discharges [10], but again, the radiation is mainly from carbon, although the inner wall of Alcator C-Mod is made of molybdenum. The situation is somewhat different in JET [11]. With deuterium puffing the radiation losses increase, but as the density increases, the plasma falls back into L-mode before the radiation losses are large enough for the divertor plasma to detach. Apparently the large tokamak JET has such small intrinsic impurity content that it usually operates with much smaller radiation losses (in standard H-mode JET has about 20% radiation only) than smaller tokamaks. Therefore, the additional loss required to reach divertor detachment is larger than what can be achieved within the density operating window.

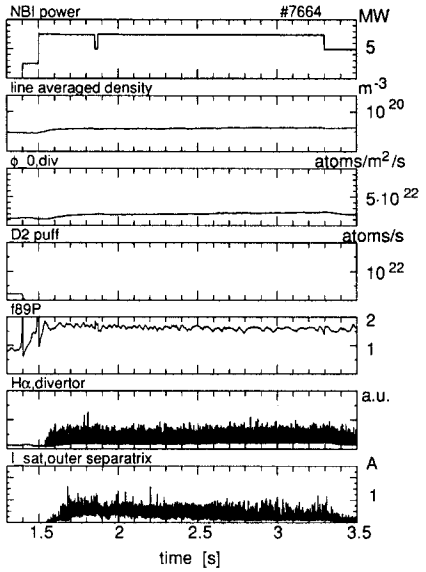

Fig. 1. Time traces for a 'standard' H-mode discharge on ASDEX Upgrade (#7664). During the neutral beam heating phase the external D_2 gas valve is switched off, and while the line averaged density (measured with a DCN interferometer along a horizontal channel in the mid-plane) stays almost constant, the divertor neutral gas flux density $\phi_{0,\mathrm{div}}$ increases by about 15% during the heating phase. The H_α-light at the outer target plate shows the type-I ELMs. The ion saturation current to the outer target near the separatrix decreases slowly, but does not show any sign of detachment. The confinement factor f_{89P} is defined as $f_{89P} = \tau_E / \tau_{ITER89P}$.

In most of the tokamaks the energy confinement worsens only slightly with deuterium puffing, except in JT-60U, where the energy confinement time drops continuously with increasing gas puff to L-mode values [9,12]. This is probably related to the divertor being not separated from the main plasma chamber at all, resulting in negligible baffling of the neutrals from the divertor region. The rather high neutral gas density around the bulk plasma probably deteriorates confinement, even though the reason for this is not yet understood [13].

For reference a standard H-mode discharge in ASDEX Upgrade, described also in [14], is shown in Fig. 1. The base parameters of this discharge and the other ASDEX Upgrade discharges to be discussed later are $I_p = 1.0$ MA, $B_t = -2.5$ T (i.e., clockwise as seen from above, ion drift towards the divertor), $q_{0.95} \sim 4$. These discharges are pumped with an effective pumping speed of about 15 m^3/s in the divertor chamber from 14 turbomolecular pumps [15]. Wall pumping is negligible during the high power heating phase. Between discharges the vacuum vessel walls are conditioned by He glow discharge cleaning (HeGDC).

At the start of neutral beam injection the external

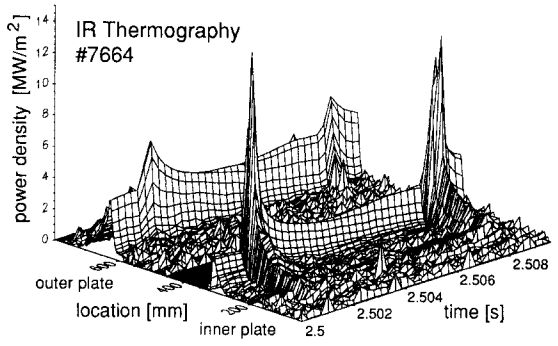

Fig. 2. Power density in the divertor during a 'standard' H-mode discharge without gas puffing (see also Fig. 1). The ELMs at 2.502 and 2.509 s result in large power bursts to the target, but also between the ELMs the power density is high.

deuterium gas valve is switched off and the line averaged density increases, reaching an equilibrium after about 300 ms. The divertor neutral gas flux density $\phi_{0,\mathrm{div}}$ is measured with ionization gauges in the divertor chamber behind the passive stabilizing coil (PSL). $\phi_{0,\mathrm{div}}$ is a measure for the neutral density, but the absolute conversion is impossible without a knowledge of the neutrals energy distribution at this location [15]. $\phi_{0,\mathrm{div}}$ does not reach an equilibrium in this scenario, but it increases steadily, by about 15% over the duration of the heating phase. The confinement factor $f_{89\mathrm{P}} = \tau_{\mathrm{E}}/\tau_{\mathrm{ITER89P}}$ (where τ_{ITER89P} is the energy confinement time according to a L-mode database confinement [16]) is about 1.6 in this phase. The H_α-signal in the outer divertor shows type-I ELMs that are also seen on the ion saturation current to the outer target plate near the separatrix, measured with flush mounted Langmuir probes [17]. The baseline of $I_{\mathrm{sat,out}}$ slowly decreases, but does not show any clear sign of detachment. The total radiation losses measured with bolometry account for about 55% of the input power, with about 15% inside the separatrix and about 10% in the divertor, i.e., below the X-point.

Fig. 2 shows the target power load measured by infrared thermography [18]. The power density increases strongly during ELMs, while between ELMs the maximum power density is still about 2.5 MW/m^2 on the inner and about 5 MW/m^2 on the outer target plate. Such power bursts would not be compatible with detached divertor operation on ITER.

As was shown before, for constant line averaged density the divertor neutral density has a long equilibration time, due to the influence of the vacuum vessel walls. In this scenario, i.e., without external deuterium flux during the NBI heating phase, the wall usually releases gas [15]. The divertor neutral density is, however, an important parameter as it influences the divertor conditions and also because it is closely linked to the mid plane edge density and the main chamber neutral density [19]. Therefore deuterium puffing in ASDEX Upgrade is always done with

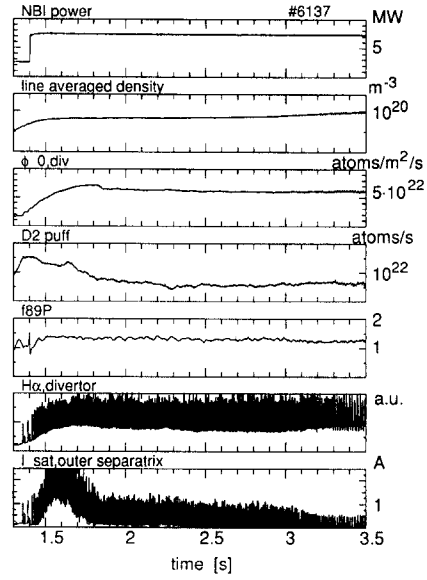

Fig. 3. Time traces for a H-mode discharge with additional D_2-puffing on ASDEX Upgrade. During the neutral beam heating phase the divertor neutral gas flux density $\phi_{0,\mathrm{div}}$ is feedback-controlled by the D_2-puff. The H_α-light at the outer target plate still shows the type-I ELMs with the base line of the signal increasing with the divertor neutral gas density. With the increase in $\phi_{0,\mathrm{div}}$, the base line of the ion saturation current near the outer separatrix drops by a factor of 8, indicating detachment between the ELMs, while the ELMs still burn through. The change in ELM frequency and the further decrease of the I_{sat} baseline are a consequence of continuous carbon influx.

feedback control of the gas valve on $\phi_{0,\mathrm{div}}$, thereby reaching steady state conditions in the divertor much more rapidly. A typical case is shown in Fig. 3, where $\phi_{0,\mathrm{div}}$ is a factor of 3 higher than in the unpuffed discharge shown in Fig. 1. Due to the large gas puff rate the confinement is a little worse, the confinement factor $f_{89\mathrm{P}}$ being about 1.4 at the start of neutral beam heating, decreasing to about 1.3. The total radiation loss is about 65% during the NBI

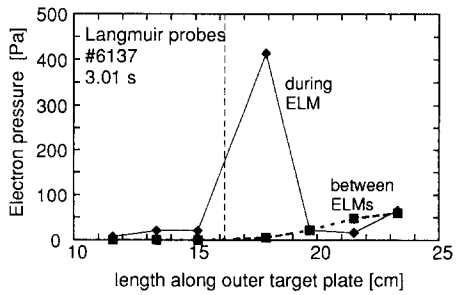

Fig. 4. Electron pressure at the outer target plate, measured with Langmuir probes. Between ELMs the pressure is negligible and the profile is flat, but during the ELM the plasma reattaches, and the pressure near the separatrix (shown by the vertical broken line) increases dramatically.

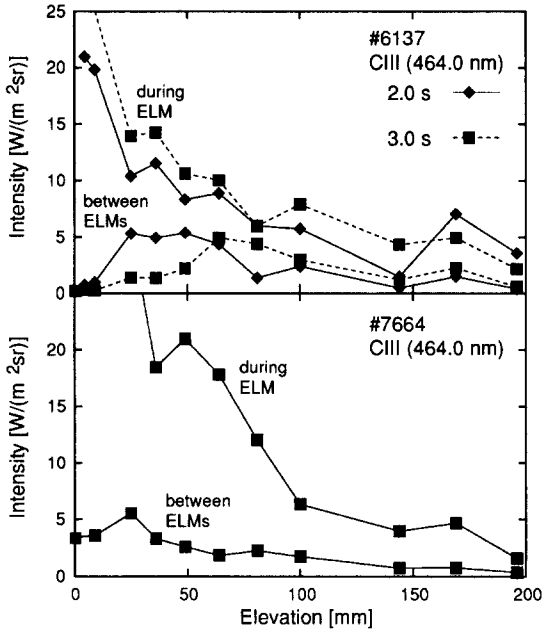

Fig. 5. CIII radiation profiles in front of the outer target plate. 'Elevation' is the distance of the line of sight from the target plate [20]. The top part of the figure shows two time slices in the deuterium puffed discharge from Fig. 3, each with profiles between and during ELMs, where the detachment between ELMs is clearly seen. The bottom part shows the profiles in the unpuffed ELMy H-mode of Fig. 1, where the plasma is attached also between ELMs.

phase, with about 20% of the total input power radiated from the divertor. The radiated power fraction inside the separatrix increases from about 25% after beam switch-on to about 30% at 3.5 s, while the X-point radiation decreases after 2.8 s. The target power flow decreases simultaneously, as can be seen in the baseline of the ion saturation current at the outer separatrix. After a strong decrease during the buildup of the divertor neutral gas flux density, when the plasma detaches, it continues decreasing, indicating a strengthening of detachment. As discussed before, in this scenario the main radiator is carbon, and the reason for the increasing radiation is a continuous carbon influx. In these deuterium-puffed discharges in ASDEX Upgrade the power load to the ICRH antenna limiters and the inner wall is rather high, resulting in enhanced sputtering of carbon.

Although the baseline of the ion saturation current at the outer separatrix is rather low, it still shows clearly the type-I ELMs, indicating that during ELMs the plasma reattaches to the target plate. This can be seen in the profile of the electron pressure measured with these probes, as shown in Fig. 4. Between the ELMs the pressure at the outer target plate is flat and almost negligible, but during an ELM it increases dramatically.

A further detachment monitor is the CIII light in front of the outer divertor target plate, measured with the divertor spectrometer [20] [1]. The upper part of Fig. 5 shows for two time points in the puffed discharge the line intensity profiles as a function of the distance from the target plate. During an ELM the highest intensity is at the target plate, and only between ELMs does the zone with the strongest CIII radiation retract from the plate. At the later time (3.0 s), the CIII-intensity in the ELM is about a factor 2 higher than at 2.0 s, but also between ELMs the detachment (due to the carbon radiation) is stronger in the sense that the radiating zone retracts even further. The bottom part of Fig. 5 shows the same signals for the discharge from Fig. 1, and here even between the ELMs the CIII radiation very close to the target plate is high.

The radiation loss by intrinsic impurities, even when enhanced by deuterium puffing, is not sufficient to reach detachment during ELMs. The main radiator in these deuterium puffed scenarios is carbon, which shows two problems. First, carbon tends to form MARFEs which can lead to disruptions and, second, it is difficult to control: it is eroded from target plates and from the walls continuously by physical and chemical sputtering, and it is not exhausted, but redeposited. Therefore, to enhance the radiation losses further, other impurities have to be seeded into the discharge.

3. Impurity seeding

Impurity seeding of discharges for creating a cold plasma mantle was proposed in the late 1970s [21,22], where it was also shown that these impurities would have a small effect on energy confinement if they were confined to the outer plasma regions. The first successful demonstration of this concept was done on the TEXTOR tokamak [23], where neon puffing was used to radiate 85% of the input power in plasmas attached to the limiter. Meanwhile such scenarios have been used in all divertor tokamaks, with different impurities. The choice of impurity is determined by two properties:

The emission rate coefficient $L_Z(T_e)$ [24] shown in Fig. 6 determines the location of the radiating zone. Concerning the dependency on electron temperature, C and N_2 are ideally suited to radiate in the rather cold scrape-off layer, but carbon has the problems mentioned above and nitrogen builds up large wall inventories, which may cause problems when steady-state operation is approached. On the other hand, N_2 is well suited for experiments lacking active pumping. The noble gases Ne and Ar radiate at higher temperatures (in this sequence), but as they recycle fully, they can be pumped and thereby be controlled. Currently Ne and N_2 are most often used in radiative scenarios.

[1] Viewing along the outer target plate.

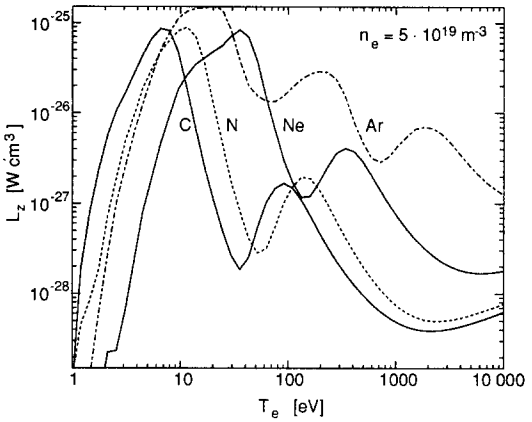

Fig. 6. Power loss emission rate coefficients from a collisional-radiative model, calculated for a density of 5×10^{19} m^{-3} [24]. The data for argon are from Ref. [49].

The first divertor tokamak experiments with Ne puffing were reported in 1994 [14,25,26], showing a strong increase of radiation. This radiation comes partly from the core region and influences the ELM behavior [25,26] in that the type-I ELMs change to type-III ELMs. JET did not succeed in detaching the divertor with Ne puffing [11]. The discharges instead returned to L-mode. With N_2, however, JET plasmas with an input power of about 15 MW can detach from the target plates, while staying in H-mode with type-III ELMs. Also in Alcator C-Mod detachment in high power H-mode discharges could be obtained only with N_2 [27,28], while JT-60U achieves detached divertor plasmas with Ne [12]. Again, JT-60U sees a strong deterioration of the energy confinement with Ne puffing. Ne puffing in DIII-D results in a strong reduction of the power flux to the target plates and a change of the ELM type (from type I to type III) [25,29].

All these experiments use simultaneous puffing of the 'seed impurity' and D_2. The first experiments with Ne on ASDEX Upgrade showed that the Ne exhaust rate increases strongly with increasing divertor neutral gas flux density $\phi_{0,\mathrm{div}}$ [26], which improves the controllability and also the radiation efficiency (increase in radiation loss normalized by the increase in Z_{eff}) increases with $\phi_{0,\mathrm{div}}$ [30]. This is a consequence of the edge density increasing with $\phi_{0,\mathrm{div}}$ [19], thereby improving the screening of Ne.

To operate impurity seeded discharges safely in the window between attached operation (with too low radiation losses) and radiative collapse (with too high radiation losses), it is required to feedback-control the impurity influx, as it is routinely done on ASDEX Upgrade [26]. With the simultaneous feedback-control of the deuterium puff (on $\phi_{0,\mathrm{div}}$) and the neon puff (on P_{rad} from a weighted sum of bolometer channels) stationary detached plasmas can be established. As under these conditions the plasma stays in H-mode, this operational mode is named Completely Detached H-mode (CDH) [31]. An example for such a discharge is shown in Fig. 7. The second frame shows the two feedback-controlled gas puffs (from absolutely calibrated piezo valves), while the third and fourth frames show the regulated parameters, the neutral gas flux density in the divertor, $\phi_{0,\mathrm{div}}$ and the total radiated power. About 95% of the total input power is radiated, with 45% (of the total input power) from the bulk plasma and 20% in the divertor. The H_α-light in the divertor shows a strong increase in the baseline (almost proportional to $\phi_{0,\mathrm{div}}$), and on top of that first the type-I ELMs, which then disappear at about 1.5 s. They are replaced by small type-III ELMs, which are not detectable with the IR thermography of the divertor target plates. At the same time the plasma detaches, as seen in the CIII light just above the outer target plate (this trace shows the first channel of the divertor spectrometer, just above the target plate, compare with Fig. 5) and in the ion saturation current at the outer separatrix, which shows a factor of three modulation in these type-III ELMs [32]. The bottom part of this figure shows the confinement factor $f_{89P} \sim 1.5$, being stationary for about 15 energy confinement times.

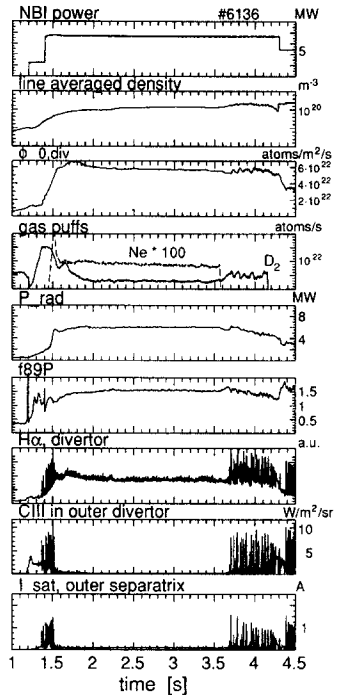

Fig. 7. Time traces for a CDH-mode discharge with feedback-controlled D_2 and Ne puffing in ASDEX Upgrade. During the neutral beam heating phase the divertor neutral gas flux density $\phi_{0,\mathrm{div}}$ is feedback-controlled by the D_2-puff, and the total radiated power P_{rad} (measured from 12 bolometer channels) by the Ne-puff. The H_α-light at the outer target plate first shows the type-I ELMs which then change to type-III ELMs. The ion saturation current near the outer separatrix and the CIII intensity just above the outer target plate drop strongly with the increase in $\phi_{0,\mathrm{div}}$, and both do not show the ELMs anymore, indicating detachment from the divertor plasma.

Accumulation of Ne in these discharges does not occur as long as sawteeth are preserved. Still, the neon contribution to Z_{eff} in the central part of ASDEX Upgrade CDH-mode discharges is about 0.7 with sawteeth and 1.2 without sawteeth, with the total Z_{eff} being about 2.7 and 3.5 respectively. Such values are far too high for ITER [1]. Recent scaling studies of the required impurity content with machine size [33], however, indicate that such radiative scenarios might be possible for ITER. Another issue in the extrapolation of CDH-mode towards ITER is the threshold power for fallback from H- to L-mode [19]. The possible power losses inside the separatrix are limited, as the power flow over the separatrix has to be above the threshold power.

4. Particle exhaust in gas-puffed plasmas

Having discussed three different operating scenarios, namely (1) 'standard' H-mode with type-I ELMs (without additional gas puff), (2) deuterium puffed H-mode and (3) detached plasma with deuterium and impurity puffing, we will discuss and compare particle exhaust in these three modes.

We investigate He- and Ne-exhaust with short gas puffs by observing the decay rate of the recycling signals [15,30]. As both gases fully recycle at walls and target plates, this decay rate is identical with the exhaust time, or the global particle confinement time τ_p^*. Experiments in plasmas without or with small external pumping indicate that both gases are not pumped by the walls [15,34] and the assumption of full recycling is justified. Absorption on the walls with short time constants (i.e., in the order of 10 ms), as it is assumed in DIII-D [35], can not be excluded, but for the interpretation of (much longer) pumping time constants this effect would not play a role. The exhaust rate, however, depends strongly on the effective pumping speed S_{eff} in the divertor chamber, and a more physical quantity is the compression factor C_i which for the species i is defined as the ratio of neutral density in the divertor chamber (i.e., at the pump duct) to the ion density in the main plasma (usually taken as the value at the plasma edge). This parameter reflects the fact, that the particle fluxes in the scrape-off layer increase from midplane towards the target plate due to the flux amplification at the plate itself. The compression, however, also depends on the leakage of neutrals out of the divertor, either in the scrape-off layer or outside the plasma. This depends on the mean free path (i.e., on the collision cross sections) and is therefore different for different species. A further useful parameter therefore is the enrichment factor

$$\eta_{He} = \frac{\left(n_{0,He}/2 \cdot n_{D_2}\right)^{div}}{\left(n_{He}/n_e\right)^{edge}}, \qquad (1)$$

where $n_{0,He}$ and n_{D_2} are the densities of helium and deuterium neutrals in the divertor chamber, n_{He} and n_e are the helium ion and the electron densities at the plasma edge in the midplane [36,37]. Using the compression factors C_i, η_{He} can also be expressed as

$$\eta_{He} = C_{He}/C_{D_2}. \qquad (2)$$

In general, η_{He} has to be determined from 4 local measurements of the respective densities. However, using a simple two-chamber model [26], one can derive an expression for C_{He} which depends on τ_p^* only:

$$C_{He} = \frac{V^{main}}{S_{eff}\tau_p^* - V^{div}} \qquad (3)$$

with V^{main} and V^{div} being the respective volume of the main plasma chamber and the (pumped) divertor chamber.

Fig. 8 shows a summary of exhaust experiments on ASDEX Upgrade. The top figure shows measured exhaust rates for Ne (in deuterium puffed H-mode discharges) and for He. The leftmost He data point is from an unpuffed H-mode, the others are from deuterium puffed H-modes and CDH-modes at two divertor neutral densities. These He decay rates have an error of about 10%, and within those error bars the decay rates for deuterium puffed H-modes and CDH-mode discharges are identical. The two data points at $\phi_{0,div} = 6 \times 10^{22}$ m^{-2} s^{-1} are from the

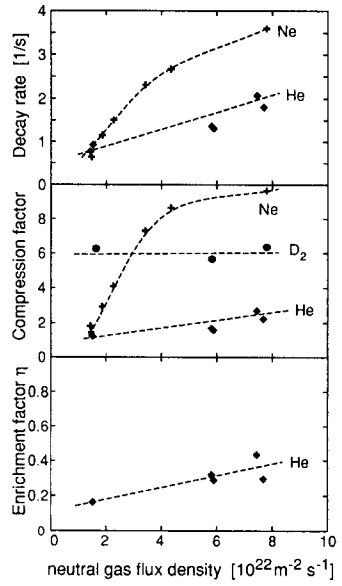

Fig. 8. Summary of exhaust experiments in ASDEX Upgrade. The top figure shows measured exhaust rates for Ne (Puffed H-mode discharges) and for He. The leftmost He datapoint is from an unpuffed H-mode, the others are from deuterium puffed H-modes and CDH-modes at two divertor neutral densities. The middle figure shows the compression factor for He and Ne (derived from τ^* with the two chamber model) and for D_2 (from local measurements). The bottom figure shows the enrichment factor for He derived from the compression factors in the figure above.

discharges shown in Figs. 3 and 7, and they are hardly distinguishable. One sees clearly, that the radiation loss in CDH-mode does not influence the exhaust rate or the divertor compression. The middle figure shows the compression factor for He and Ne (derived from τ_p^*; with the two chamber model) and for D_2 (from local measurements). Generally we find that C_{Ne} is much larger than C_{He}, and the ratio is even larger than it is for the exhaust rates. Because $S_{eff,Ne}$ is smaller than $S_{eff,He}$ [15] this large difference in the compression factors becomes somewhat reduced in the exhaust rates, as is seen in this figure. The bottom figure shows the enrichment factor for He derived from the compression factors in the figure above. At $\phi_{0,div} = 6 \times 10^{22}$ m^{-2} s^{-1} compression factor and enrichment in the deuterium puffed H-mode are actually larger than in the corresponding CDH-mode discharge, but still within the error bars the two scenarios show identical values. In general we find that η_{He} in both types of puffed discharges is larger than 0.3, which is above the value of 0.2, required by the current ITER design [1].

A similar relation between compression and average plasma density (and correspondingly increasing divertor neutral gas density) has been seen on TdeV [38,39]. C_{He} and C_{D_2} both increase with density, resulting in a constant $\eta_{He} = 0.17$, independent of density, heating method, and for attached as well as for detached divertor plasmas.

The question arises what is the reason for the improvement of compression (or divertor retention) with increasing divertor neutral gas flux density. The increase in $\phi_{0,div}$ is achieved by an external D_2 flux Γ_{ext}. For a stationary case this has to be equal to the pumped flux Γ_{pump} which can be written as $\Gamma_{pump} = n_{0,div} S_{eff}$ with $n_{0,div}$ being the neutral density in the divertor chamber. Therefore, for a constant pumping speed S_{eff}, externally induced gas flow in the scrape-off layer and divertor neutral density (or flux density) are directly coupled, and it can not be decided which parameter is the determining one. However, by varying the pumping speed, a series of CDH-mode discharges has been performed with identical $\phi_{0,div}$, but strongly varying external gas flow [40]. As the discharges were practically identical, and also the divertor retention was practically the same, it was concluded that it is not the externally induced gas flux, but $\phi_{0,div}$, or another parameter directly linked to it that is important. As mentioned before, $\phi_{0,div}$ is linked to the midplane neutral density and the midplane separatrix density [19], but it is also a measure for a neutral gas reservoir in the divertor chamber (below the small baffle ring and the passive stabilizer loop (PSL)), from which neutrals stream again from the side into the lower part of the scrape-off layer. There these neutrals are ionized and contribute strongly to the flux enhancement in front of the target plate. It is thought that this flux enhancement is responsible for the compression improving with $\phi_{0,div}$. 'Puff and Pump' experiments in DIII-D [35,41], however, show that the Ne compression depends on strength and location of the external gas puff. Although in the latest series of experiments most of the plasma parameters are almost identical, the ELM behavior varies considerably between the different discharges, and it is not clear how this affects the compression. At present the reason for these differences in impurity retention between ASDEX and DIII-D is not yet understood, but the geometrical differences between the two experiments might be the reason, as will be discussed later.

5. 2D modelling of divertor compression

The experimental results show an increase of compression with the divertor neutral gas flux density and a better compression for Ne than for He. As impurity retention in the divertor depends on a delicate balance of different forces and on two-dimensional flow patterns, such processes can only be interpreted with the help of 2D-codes.

We have used the code package B2-EIRENE [42,43], based on the multifluid plasma code B2 [44] and the Monte Carlo neutral particle code EIRENE [45]. With this package a typical CDH-scenario has been modelled [46], trying to fit many of the experimental signals. These simulations included 19 plasma species (all ionization stages of D, He, C, Ne) and a model for chemical sputtering of carbon. By varying the divertor neutral gas density,

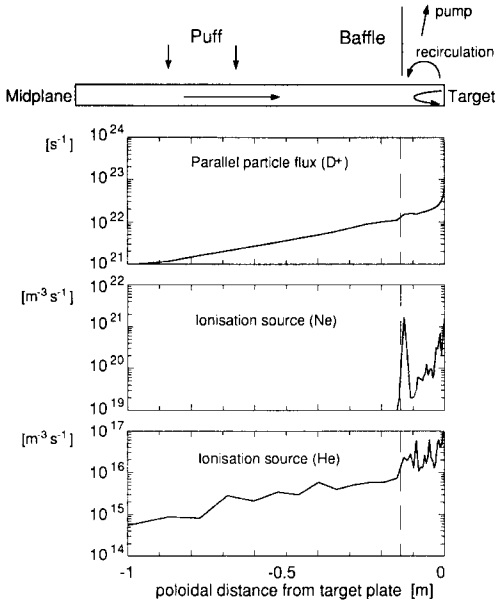

Fig. 9. The top part of this figure shows a simplified model of the fluxes in scrape-off layer and divertor, while the graphs show results from B2-EIRENE modelling. The first graph shows the deuterium ion flux towards the outer target plate, which shows a step of a factor 2 at the baffle (where the recirculation fluxes start contributing) and the large increase directly in front of the target plate (internal recycling). The two bottom graphs show the location of the ionization of Ne and He, indicating that He with its much longer ionization mean free path leaks out of the divertor region much stronger.

both effects seen in the experiment (compression improving with $\phi_{0,\mathrm{div}}$ and better compression of Ne than of He) have been reproduced by the code [47]. Analysis of the runs shows the importance of two-dimensional flow patterns in the divertor region, but the main effect comes from a decreasing mean free path of the neutrals recycling from the target plate or 'recirculating' from the divertor chamber. In the top part of Fig. 9 a simple model of the particle fluxes is shown. The external gas puff in the main chamber induces a flow in the scrape-off layer, directed towards the target plates (for simplicity only one divertor leg is shown here). At the target plate the ions are neutralized and can either leave the plasma towards the divertor chamber or return into the scrape-off layer, where they are ionized and stream back towards the target plate. Most of the neutrals escaping into the divertor chamber return into the scrape-off layer (recirculation), only a small fraction of them is pumped. Both the internal recycling and the recirculation enhance the plasma flow in the scrape-off layer strongly and can counterbalance thermal forces that would drive ions back towards the main chamber. This simple picture can also be found in the results of the B2-EIRENE modelling. The top graph in Fig. 9 shows the D^+ flux in the outer part of the scrape-off layer. At the baffle (which should cut off the recirculation) we see a strong (factor of 2) increase of the ion flow towards the target, as expected. The lower graphs show the location of the ionization of Ne and He, and one sees clearly that Ne has a much shorter ionization mean free path than He, practically all N and atoms are ionized in this region of enhanced particle flow. He not only has a larger mean free path, but also experiences charge exchange which can let it escape further as neutral, and therefore a large fraction of it is reionized above the baffle, where it can more easily enter into the main plasma.

With this picture it is also clear that higher $\phi_{0,\mathrm{div}}$ (and higher divertor density) improves the compression of He, as the mean free path decreases. This simple model even indicates possible explanations of the different impurity transport behavior in DIII-D. The Advanced Divertor Baffle is much tighter than the baffle ring in ASDEX Upgrade, and its width has been optimized for pumping (and retention) of deuterium. Therefore this 'step' in the flux enhancement is located much closer to the target, and especially much closer than the ionization mean free path of Ne or He. That means, a large fraction of Ne (and He) is ionized in the scrape-off layer far above the enhanced deuterium flux region, and might be much more sensitive to changes in the (smaller) externally induced deuterium flow. However, only detailed 2D modelling of DIII-D can give a detailed answer.

6. Conclusions

Deuterium puffing increases the radiation losses strongly, and can result (between ELMs) in detached divertor plasmas. However, in this scenario carbon is the main radiating species, and therefore it is usually connected to a MARFE at the X-point. There is a intrinsic influx of carbon from physical and chemical sputtering at the walls and divertor target plates, which depends solely on particle fluxes to these surfaces and on the local electron temperature, and can therefore not be controlled directly.

In large tokamaks such as JET, the increase in radiation loss from intrinsic impurities is not sufficient to cause detachment. The plasma instead falls back into L-mode when the plasma density is increased too strongly. Generally, a deterioration of the confinement with the additional deuterium puff is seen.

Impurity seeding can greatly increase the radiation loss, resulting in detachment even during ELMs. Moreover, in these plasmas with a small power flux over the separatrix (i.e., close to the L–H threshold) the ELMs switch from large type-I ELMs (which could not be tolerated in ITER) to the more benign type-III ELMs. The optimum choice of the impurity species depends on the plasma parameters, but Ne (in ASDEX Upgrade, DIII-D, JT-60U) as well as N_2 (in JET, and Alcator C-mod) have been used successfully for achieving detached divertor plasmas. Ne as a recycling gas can be controlled very efficiently, and this led to the establishment of CDH-mode in ASDEX Upgrade, where the total radiation loss is feedback-controlled by the Ne influx. Controllability of Ne is improved with additional deuterium puffing.

The exhaust rate of He is also improved with additional gas puffing, although the divertor neutral gas flux density $\phi_{0,\mathrm{div}}$ and the recirculating flux in the divertor chamber are the more meaningful parameters. The high radiation losses in CDH-mode and the detached divertor operation do not impair the He compression in the ASDEX Upgrade divertor. This is probably because detachment in CDH-mode is still moderate in the sense that the detachment front is still close to the target plate and has not yet retracted far from the target plate. Only with such strong detachment the neutrals would escape from the divertor chamber and compression should deteriorate.

2D modelling reproduces the experimental results on He- and Ne-compression and helps in explaining them. Modelling of compression in different divertor geometries shows clearly the importance of geometry [48], and a simple model (backed up by the 2D modelling results) offers some clues to the differences in Ne transport in the scrape-off layer of ASDEX Upgrade and DIII-D. However, further modelling and analysis of the code results is necessary to reach a deeper understanding of particle exhaust in divertor experiments.

Acknowledgements

The authors gratefully acknowledge the help of S. Allen (DIII-D), B. Lipschultz (Alcator C-Mod), N. Asakura and K. Itami (JT-60U), J.-L. Gauvreau (TdeV), and G.

Matthews (JET) in providing additional information on the results of the respective experiments.

References

[1] G. Janeschitz, ITER-JCT, and Home Teams, Plasma Phys. Controlled Fusion 37 (1995) A19.
[2] E.J. Doyle, R.J. Groebner, K.H. Burrell, P. Gohil, T. Lehecka et al., Phys. Fluids B3 (1991) 2300.
[3] A. Kallenbach, R. Dux, H.-S. Bosch, K. Büchl, J. Fuchs et al., Plasma Phys. Controlled Fusion 38 (1996) 2097.
[4] G.F. Matthews, J. Nucl. Mater. 220–222 (1995) 104.
[5] D. Reiter, G.H. Wolf and H. Kever, Nucl. Fusion 30 (1990) 2141.
[6] T.W. Petrie, D.N. Hill, D. Buchenauer, A. Futch, C. Klepper et al., in: Europhysics Conference Abstracts (Proc. 18th EPS Conf. on Controlled Fusion and Plasma Physics, Berlin, 1991), ed. P. Bachmann and D.C. Robinson, Vol. 15C, part III (EPS, Geneva, 1991) p. 237.
[7] T.W. Petrie, D. Buchenauer, D.N. Hill, C. Klepper, S. Allen et al., J. Nucl. Mater. 196–198 (1992) 848.
[8] T.W. Petrie, D.N. Hill, S.L. Allen, N.H. Brooks, D. Buchenauer et al., 'Radiative divertor experiments in DIII-D with D_2 injection, GA-A21879, May 1995', submitted to Nucl. Fusion.
[9] N. Asakura, N. Hosogane, K. Itami, S. Tsuji, M. Shimada et al., in: Proc. 15th Int. Conf. on Plasma Physics and Controlled Nuclear Fusion Research, Sevilla 1994, Vol. I (IAEA, Vienna, 1995) p. 515.
[10] B. Lipschultz, J. Goetz, B. LaBombard, G.M. McCracken, J.L. Terry et al., J. Nucl. Mater. 220–222 (1995) 50.
[11] The JET Team, presented by G.F. Matthews, Plasma Phys. Controlled Fusion 37 (1995) A227.
[12] K. Itami and the JT-60 Team, Plasma Phys. Controlled Fusion 37 (1995) A255.
[13] S.-I. Itoh, K. Itoh and A. Fukuyama, J. Nucl. Mater. 220–222 (1995) 117.
[14] M. Kaufmann, N. Lackner, V. Mertens, J. Neuhauser, H. Zohm et al., in: Plasma Physics and Controlled Nuclear Fusion Research 1994, Vol. 1 (IAEA, Vienna, 1995) p. 491.
[15] H.-S. Bosch et al., 'Particle exhaust studies in ASDEX Upgrade', to be submitted to Nucl. Fusion.
[16] P.N. Yushmanov, T. Takizuka, N.S. Riedel, O.J.W.F. Kardaun, J.G. Cordey et al., Nucl. Fusion 30 (1990) 1999.
[17] M. Weinlich et al., 'Flush mounted Langmuir probes in an oblique magnetic field', to be submitted to Phys. Plasmas.
[18] A. Herrmann, W. Junker, K. Günther, S. Bosch, M. Kaufmann et al., Plasma Phys. Controlled Fusion 37 (1995) 17.
[19] H.-S. Bosch, O. Gruber, G. Haas, A. Kallenbach, M. Kaufmann et al., Plasma Phys. Controlled Fusion 38 (1996) 1493.
[20] G. Lieder, B. Napiontek, R. Radtke, A.R. Field, G. Fussmann et al., in: Europhysics Conf. Abstracts (Proc. of the 20th EPS Conf. on Controlled Fusion and Plasma Physics, Lisbon, 1993), ed. J.A. Costa Gabral, M.E. Manso, F.M. Serra and F.C. Schüller, Vol. 17C, part II (EPS, Geneva, 1993) p. 579.
[21] A. Gibson and M.L. Watkins, in: Proc. 8th European Conf. on Controlled Fusion and Plasma Physics, Prague, Vol. I (1977) p. 31.
[22] K. Lackner and J. Neuhauser, in: Proc. IAEA Techn. Comm. Meeting on Divertors and Impurity Control, Garching, 1981, ed. M. Keilhacker and U. Daybelge (IAEA, Vienna, 1981) p. 58.
[23] U. Samm, G. Bertschinger, P. Bogen, J.D. Hey, E. Hintz et al., Plasma Phys. Controlled Fusion 35 (1993) B167.
[24] H. P. Summers, Technical Report Jet-IR(94)06, JET Joint Undertaking, Culham, 1994.
[25] D.N. Hill, S. Allen, N.H. Brooks, D. Büchenauer, J.W. Cuthbertson et al., in: Proc. 15th Int. Conf on Plasma Physics and Controlled Nuclear Fusion Research, Sevilla 1994, Vol. I (IAEA, Vienna, 1995) p. 499.
[26] A. Kallenbach, V. Mertens, R. Dux, M. Alexander, K. Behringer et al., in: Plasma Physics and Controlled Nuclear Fusion Research 1994, Vol. 2 (IAEA, Vienna, 1995) p. 105.
[27] J.A. Goetz, C. Kurz, B. LaBombard, B. Lipschultz, A. Niemczewski et al., Phys. Plasmas 3 (1996) 1908.
[28] B. Lipschultz,J.A. Goetz, B. LaBombard, G.M. McCracken, H. Ohkawa, Y. Takase and J.L. Terry, these Proceedings, p. 771.
[29] S.L. Allen, A.S. Bozek, N.H. Brooks, D.A. Buchenauer, K H. Burrell et al., Plasma Phys. Controlled Fusion 37 (1995) A191.
[30] A. Kallenbach, R. Dux, V. Mertens, O. Gruber, G. Haas, et al., Nucl. Fusion 35 (1995) 1231.
[31] O. Gruber, A. Kallenbach, M. Kaufmann, K. Lackner, V. Mertens et al., Phys. Rev. Lett. 74 (1995) 4217.
[32] J. Neuhauser, M. Alexander, G. Becker, H.-S. Bosch, N. Büchl et al., Plasma Phys. Controlled Fusion 37 (1995) A37.
[33] G. Matthews et al., these Proceedings, p. 450.
[34] R. Dux, A. Kallenbach, M. Bessenrodt-Weberpals, K. Behringer, H.-S. Bosch et al., Plasma Phys. Controlled Fusion 38 (1996) 989.
[35] M. Schaffer, M.R. Wade, R. Maingi, P. Monier-Garbet, W.P. West, D.G. Whyte, R.D. Wood and M.A. Mahdavi, these Proceedings, p. 585.
[36] M. Shimada, M. Nagami, K. Ioki, S. Izumi, M. Maeno et al., Phys. Rev. Lett. 47 (1981) 796.
[37] J.C. De Boo, N.H. Brooks, J.S. De Grassie, M.A. Mahdavi, N. Ohyabu et al., Nucl. Fusion 22 (1982) 572.
[38] J.-L. Gauvreau, 'Divertor He retention and pumping under detached plasma conditions in TdeV', 3rd Int. He-Workshop, Charleston, SC, USA, Sept. 1995.
[39] N. Richard, B. Terreault, E. Haddad, J. Gunn, G. Abel, S. Chiu, J.-L. Gauvreau, H.H. Mai and W.W. Zuzak, these Proceedings, p. 760.
[40] H.-S. Bosch, R. Dux, G. Haas, A. Kallenbach, M. Kaufmann et al., Phys. Rev. Lett. 76 (1996) 2499.
[41] M.J. Schaffer, D.G. Whyte, N.H. Brooks, J.W. Cuthbertson, J. Kim et al., Nucl. Fusion 35 (1995) 1000.
[42] D. Reiter, P. Boerner, B. Kueppers, M. Baelmans, and G. Maddison, Technical Report 428/90-8/FU-D, NET, EURNPOM, 1990.
[43] R. Schneider, D. Reiter, H.P. Zehrfeld, B. Braams, M. Baelmans et al., J. Nucl. Mater. 196–198 (1992) 810.
[44] B.J. Braams, A Multi-Fluid Code for Simulation of the Edge Plasma in Tokamaks, NET Report No. 68, January 1987 (EUR-FU/XII-80/87/68).
[45] D. Reiter, Technical Report Jül-2599, NFA Jülich, Germany, 1992.

[46] R. Schneider, D. Coster, J. Neuhauser, H.-S. Bosch, J. Fuchs et al., in: Europhysics Conference Abstracts (Proc. 22nd EPS Conf. on Controlled Fusion and Plasma Physics, Bournemouth, 1995), ed. B. Keen, P. Stott, and J. Winter, Vol. 19C, part IV (EPS, Geneva, 1995) p. 285.
[47] D.P. Coster et al., these Proceedings, p. 690.
[48] R. Schneider, H.-S. Bosch, J. Neuhauser, D. Coster, K. Lackner and M. Kaufmann, these Poceedings, p. 701.
[49] K. Behringer, private communication, 1996.